

# QSO Lensing Magnification by Galaxies and Galaxy Groups

Antonio C. C. Guimarães<sup>1</sup>★, Adam D. Myers<sup>2</sup> and Tom Shanks<sup>1</sup>

<sup>1</sup> Department of Physics, University of Durham, Science Laboratories, South Road, Durham, DH1 3LE, U.K.

<sup>2</sup> Department of Astronomy, University of Illinois, 1002 W Green Street, Urbana, IL 61801, USA

23 May 2019

## ABSTRACT

We develop a new and more realistic approach to calculate QSO-galaxy and QSO-group of galaxies correlations due to gravitational lensing. We have simulated both the matter and light (galaxy) distributions in a wedge of the universe and calculated the gravitational lensing magnification caused by the mass along the line of sight of galaxies and galaxy groups identified in sky surveys. A large volume redshift cone containing cold dark matter particles mimics the expected cosmological matter distribution in a flat universe with low matter density and a cosmological constant. We generate a mock galaxy catalogue from the matter distribution and identify thousands of galaxy groups in the luminous sky projection. We calculate the expected magnification around galaxies and galaxy groups and then the induced QSO-lens angular correlation due to magnification bias. This correlation is an observable and can be used to estimate the average mass of the lens population and also make cosmological inferences. We also use analytic calculations and various analysis to compare the observational results with theoretical expectations for the cross-correlation between faint QSOs from the 2dF Survey and nearby galaxies and groups from the APM and SDSS EDR. The observed QSO-lens anti-correlations are stronger than the predictions for the cosmological model used. This suggests that there could be unknown systematic errors in the observations and data reduction, or that the model used is not adequate. If the observed signal is assumed to be solely due to gravitational lensing then the lensing is stronger than expected, due to more massive galactic structures or more efficient lensing than simulated.

**Key words:** Galaxies: clustering — Cosmology: gravitational lensing — Methods: numerical, semi-analytical — Large-scale structure of Universe

## 1 INTRODUCTION

It is now very well established that mass concentrations on the line of sight of distant sources act as gravitational lenses distorting their image. One of the effects is the shear of the image and that can be easily observed in drastic cases (strong lensing), or statistically when the lensing is weak. The other effect is the magnification of sources. Since lensing due to a matter overdensity enlarges the solid angle of the source and conserves its surface brightness, it can bring to view sources that would be too faint to observe in a magnitude limited survey, but at the same time it dilutes their population density. This phenomenon receives the name of magnification bias, and the two competing trends it engenders can give origin to both positive correlation or

anti-correlation between populations of objects with very distinct redshift separation.

Several groups have measured background-foreground angular correlation between populations of distant QSOs and nearby galaxies or galaxy groups (see Bartelmann & Schneider 2001 for a review, and Guimarães et al. 2001 for a compilation of several results). In particular, Croom & Shanks (1999) found a lack of faint QSOs around galaxy groups and interpreted the anti-correlation signal as due to gravitational lensing. Myers et al. (2003) found that the lack of QSOs around galaxy groups persists in larger samples, comparing QSOs taken from the 2dF QSO Redshift Survey (Croom et al. 2004) to galaxies taken from the APM galaxy survey (Maddox et al. 1990) and the SDSS EDR (Stoughton et al. 2002). Using a simple analysis that estimates an effective mass for the groups, both Croom & Shanks (1999) and Myers et al. (2003) find values that imply a high density universe ( $\Omega_m \gtrsim 1$ ).

★ E-mail: antonio.guimaraes@durham.ac.uk

Gaztañaga (2003) finds a strong positive cross-correlation between bright QSOs and galaxies from the SDSS EDR, to which he suggests the interpretation of a large anti-bias ( $b \approx 0.1$ ) on small scales. A similar result is put forward by Myers et al. (2004) from the strong anti-correlation found between faint 2dF QSOs and APM and SDSS EDR galaxies.

Both interpretations – high  $\Omega_m$  or high anti-bias – are allowed by the underlying lensing theory, where the background-foreground cross-correlation due to magnification bias depends linearly on the mass density of the universe and on an integration over the mass power spectrum. If we treat the two possible explanations independently, the high  $\Omega_m$  interpretation acts by increasing the overall lensing weighting factor, whereas the low  $b$  interpretation acts by increasing the lens mass. Of course both routes are not independent, since we expect higher clustering for a denser universe. Nevertheless, the results from these works are extreme, and at face value are in discordance with other observations. Although the errors from the referred works on the estimate of the universe matter density parameter and galaxy bias are large, these results motivate a more elaborate analysis of the data.

The cross-correlation between galaxies or groups with QSOs offers a direct opportunity to study and quantify gravitational magnification and the masses of the foreground population of lenses. We have made a new approach to the problem by simulating both the matter and light (galaxy) distributions. We use a large-scale simulation of the large-scale structure of the universe and a mock galaxy catalogue generated from the former to compute the gravitational magnification due to the mass associated with galaxies and galaxy groups. We use the observational results of Myers et al. (2003 & 2004) as study cases, that is, we seek to emulate the parameters of these works in our simulations and calculations.

In Section 2 we describe how we generate a simulated matter and galaxy distribution, how we identify groups of galaxies in the mock catalogue, and test the simulation against results from real galaxy surveys. In Section 3 we construct magnification maps for the simulated matter distribution, and in Section 4 we calculate the magnification around galaxy and galaxy groups, and the corresponding QSO-lens cross-correlation. In Section 5 we present an analytic approach to the cross-correlation calculation and compare it with the results from the mass-light simulation.

We show how the cross-correlation can be used to estimate the average mass of the foreground lenses in Section 6 and also compare the mass estimated from the lensing results with the mass obtained directly from the matter distribution simulation. We discuss our results in Section 7.

## 2 MASS AND LIGHT DISTRIBUTIONS

We generated a simulation of the matter distribution in a 10 by 75 degree<sup>2</sup> segment of the universe centred at one observer at zero redshift and extending to  $z = 1$ . We use the output of the Hubble Volume simulation (Frenk et al. 2000) that has  $10^9$  particles of mass  $M_{part} = 2.25 \cdot 10^{12} h^{-1} M_\odot$  in a periodic  $3000^3 h^{-3} \text{Mpc}^3$  box. We choose the “concordance model” simulation, which has  $\Omega_M = 0.3$ ,  $\Omega_\Lambda = 0.7$ ,

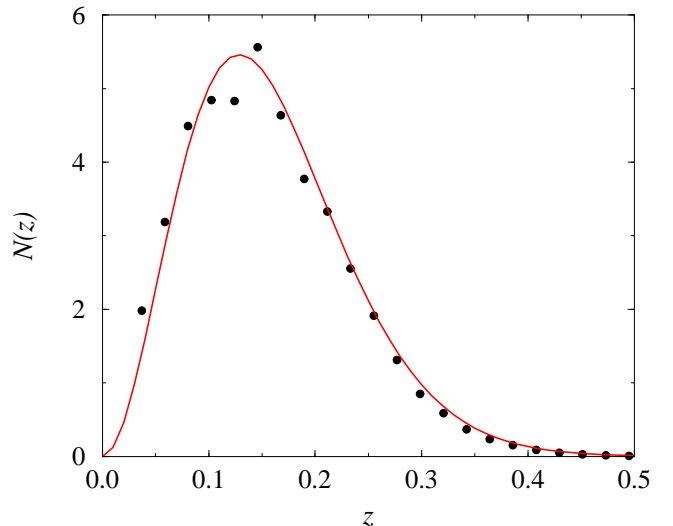


**Figure 1.** Galaxy redshift distribution. Circles are for the mock catalogue and the solid line is for expression (1).

$\Gamma = 0.21$ ,  $\sigma_8 = 0.90$ , initial fluctuations generated by CMB-FAST, and force resolution of  $0.1 h^{-1} \text{Mpc}$ .

Our simulation of the matter distribution does not incorporate the evolution of the density fields, but this shortcoming is not very relevant for our purposes since we are interested in lensing by structures at small redshift ( $z < 0.3$ ). Structures at larger redshifts, where evolution could be important, act mostly as noise for the lensing signal generated by the structures at small redshifts, since the large physical separation guarantees that they are uncorrelated. One could incorporate evolution by using the light cone output of the Hubble Volume Simulation, but so far no one has created a galaxy mock catalogue from it.

We generated a mock galaxy catalogue using the simulated mass density field and adopting a bias prescription for the galaxy population. We used the code of Cole et al. (1998), bias model 2, which is a 2-parameter model based on the final density field. The mock catalogue generated has  $4 \cdot 10^5$  galaxies magnitude limited to  $B < 20.4$ , mean redshift  $\bar{z} = 0.15$ , and redshift distribution displayed in Figure 1. This distribution is well described by the expression for galaxy redshift distributions given by Baugh and Efstathiou (1993), with  $\beta = 1.5$  and  $z_* = \bar{z}/1.412$ :

$$N(z) = \frac{\beta z^2}{z_*^3 \Gamma(\frac{3}{\beta})} \exp \left[ -\left( \frac{z}{z_*} \right)^\beta \right]. \quad (1)$$

Following Myers et al. (2003), we use the Turner and Gott (1976) algorithm to select groups of galaxies from our mock galaxy catalogue. The algorithm groups galaxies on the basis of their angular density on the plane of the sky, ignoring the redshift coordinate. About 45 per cent of groups with 7 or more members identified by the Turner & Gott algorithm have at least 7 members that are physically grouped (rather than being chance alignments along the line of sight), though 95 per cent of “Turner & Gott groups” with 7 or more members trace at least one or more triplets of physically-grouped galaxies (Myers 2003). Whether the groups identified by the Turner & Gott algorithm are physically associated or not, they certainly always represent dense

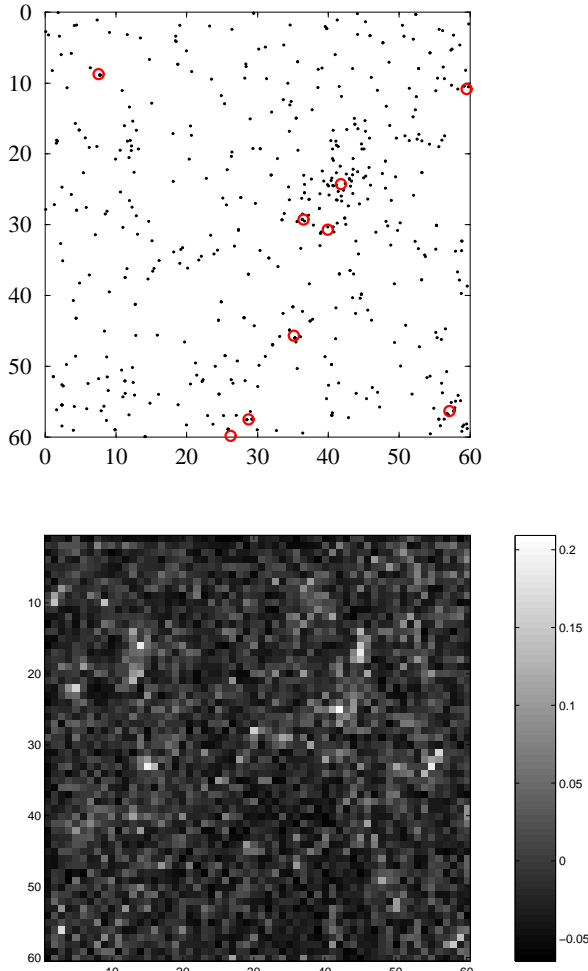


**Figure 2.** Top panel: galaxies (dots) and groups with 7 or more members (circles indicate the group centre) in a  $60 \times 60$  arcmin $^2$  sky patch. Bottom panel: convergence map in the same region for a source population at  $z = 1$ .

projections of galaxies along the line-of-sight, which should be hot-spots for lensing.

The top panel of Figure 2 shows a  $1 \times 1$  degree $^2$  projection of the simulated galaxy catalogue and the position of groups with 7 or more members identified in it. One can observe some correlation between the position of groups and regions of high convergence (therefore magnification) in the lower panel of Figure 2. The next Section will discuss how the lensing map is generated.

Not all of galaxies that are present in this patch of sky shown in Figure 2 of the mock catalogue are visible in the projection because many occupy the same position. This fact is a consequence of the low mass resolution of the N-body simulation. Because the mass particles are very massive there are too few of them at small redshifts in relation to the number of galaxies. Therefore the galaxy mock code attributes more than one galaxy to some mass particles, which explains why in the top panel of Figure 2 the groups of seven or more members and the overall sky patch appear to have fewer galaxies than expected.

The low mass resolution, and the group identification

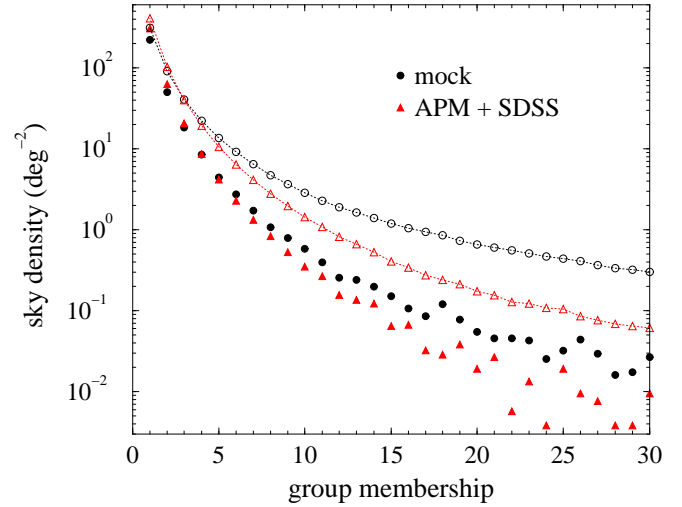


**Figure 3.** Sky density of galaxy groups identified in 2D for mock catalogue and APM + SDSS. Filled symbols are for simple membership (exactly  $N$  galaxies), and open symbols connected by lines are for groups with *at least*  $N$  galaxies.

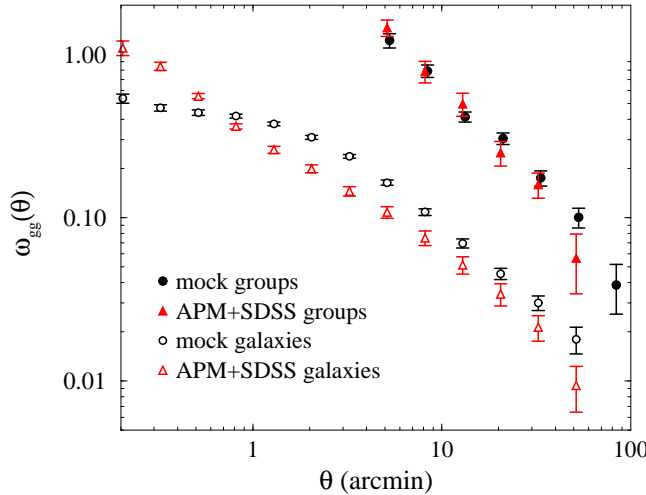
algorithm based on friend-of-friends, which identifies neighbouring galaxies inside a given radius, induce a higher identification of groups than would be expected. Assigning the same coordinates to more than one galaxy may yield a false group identification. Figure 3 shows the group density on the sky as a function of group membership. The sky density for groups with 7 or more members is  $6.5 \text{ deg}^{-2}$ , which is larger than that obtained from real data (APM + SDSS),  $3.8 \text{ deg}^{-2}$ . This discrepancy may be relevant for the objectives of this paper and reveals that the galaxies in the mock catalogue form more groups than what is observed, even though they have comparable sky density ( $540 \text{ deg}^{-2}$  for observed galaxies and  $530 \text{ deg}^{-2}$  for mock galaxies). One way to compensate for this discrepancy is to assume that the real group population is the one with same sky density as the observed. Mock groups with 9 or more members have this property as compared to observed groups with 7 or more members, and we will use those in some of our calculations, however the difference is small.

Figure 4 shows the angular auto-correlation for galaxies and groups with 7 or more members, comparing the mock catalogue with a combination of the APM and SDSS results. Mock galaxies have a lower angular auto-correlation than real galaxies for separation less than 1 arcmin (below the simulation resolution), and a somewhat higher one for larger separation. Groups with 7 or more members identified in the mock catalogue have comparable clustering to groups detected in the APM survey and SDSS.

### 3 LENSING MAPS

The full knowledge of the mass distribution between the observer at  $z = 0$  and a source distribution at high redshift allows us to calculate the gravitational lensing of sources by the intervening mass inhomogeneities.

We first calculate the convergence map generated by the mass distribution for a source surface at  $z = 1$ , using



**Figure 4.** Angular auto-correlation for galaxies and galaxy groups with 7 or more members. Errors are field-to-field.

$$\kappa(\theta) = \frac{\Sigma(\theta)}{\Sigma_{cr}}, \quad (2)$$

summed over all mass particles in the simulation.  $\Sigma(\theta)$  is the surface density of one mass particle in one angular cell of the grid adopted and

$$\Sigma_{cr} = \frac{c^2}{4\pi G} \frac{D_s}{D_d D_{ds}}, \quad (3)$$

where  $D_s$  is the angular-size distance to the source,  $D_d$  is the angular-size distance to the mass particle (deflector), and  $D_{ds}$  is the angular-size distance from the source to the mass particle.

Another expression commonly used to calculate the convergence in a cosmological context is

$$\kappa(\theta) = \int_0^{y_\infty} W(y) \delta(\theta, y) dy, \quad (4)$$

where  $\delta$  is the density contrast,  $y$  is a comoving distance,  $y_\infty$  is the comoving distance to the horizon, and  $W(y)$  is a lensing weighting function

$$W(y) = \frac{3}{2} \left( \frac{H_o}{c} \right)^2 \Omega_m \int_y^{y_\infty} \frac{G_a(y')}{a(y)} \frac{f_K(y' - y) f_K(y)}{f_K(y')} dy'. \quad (5)$$

Expression (2) is equivalent to (4) if we subtract from the former a term corresponding to the convergence of a free path (no intervening mass), i.e.  $\delta(\theta, y) = -1$ , on the second expression. This term is usually called  $\kappa_{min}$  and is small compared to the value of the convergence around the regions of interest (high mass concentration). That is the way we calculated the convergence. We used the additivity of (2) and calculated it for each mass particle in the simulation, normalizing the final field so that it has zero mean,  $\langle \kappa(\theta) \rangle = 0$ .

The approach used to calculate the convergence uses the Born approximation, which it is a good one for the lensing systems and resolution level that we use here (see Jain, Seljak and White 2000, and Vale and White 2003).

Our maps use a grid of  $1 \times 1$  arcmin $^2$  cells, which is appropriate for the resolution of the matter distribution simulation used and produces an effective smoothing on this

scale. The convergence map produced has minimum value  $\min[\kappa(\theta)] = -0.065$ , and maximum value  $\max[\kappa(\theta)] = 0.92$ , which indicates that we are probing regions where departures from the weak lensing regime,  $\kappa \ll 1$ , may be important.

The magnification map is related to the convergence  $\kappa$  and shear  $\gamma$  by

$$\mu = \frac{1}{|(1 - \kappa)^2 - \gamma^2|}, \quad (6)$$

We can assume the shear to be negligible for the purpose of the magnification calculation in the circumstances of interest here – magnification around galaxy group or cluster centres. In fact, for a NFW or SIS profile the shear will only become important in expression (6) very close to the centre, or closer than we can probe given the relative poor resolution of our mass simulation on small scales. Equation (6) reduces then to

$$\mu = \frac{1}{(1 - \kappa)^2}, \quad (7)$$

and if  $\kappa \ll 1$  (weak lensing) then it can be further simplified to

$$\mu = 1 + 2\kappa. \quad (8)$$

We calculated the magnification using both expressions (7) and (8), which already allows us to see some departure from the weak lensing linear regime. Expression (8) directly yields a null mean field for the magnification map since  $\langle \mu(\theta) \rangle = 0$ , but the same does not occur with expression (7). It is necessary to renormalize the magnification map so that  $\langle \mu(\theta) \rangle = 1$ . One can impose this condition by the means of two transformations

$$\mu(\theta) \rightarrow \mu(\theta)/\bar{\mu}, \quad (9)$$

or

$$\mu(\theta) \rightarrow \mu(\theta) - (\bar{\mu} - 1), \quad (10)$$

where  $\bar{\mu}$  is the mean value of the non-normalized magnification map. For our simulation we obtained  $\bar{\mu} = 1.0051$ , and the difference between the two renormalizations is negligible for our results here.

The importance of considering departures from the weak lensing approximation has been highlighted by Barber and Taylor (2003), and Takada and Hamana (2003).

#### 4 MAGNIFICATION AROUND LENS CENTRES AND QSO-LENS CROSS-CORRELATION

We used our magnification maps and the galaxy groups identified in the galaxy mock to calculate the average magnification in annular regions around group centres – see Figure 5. One can observe that the weak lensing approximation underestimates the average magnification, and that there is a strong dependence of the magnification on group membership. Error bars are standard deviations from the mean value considering total sampling, i.e. all cells from the grid are probed. A more realistic error estimate for an observational setting would consider a more sparse sampling. A rough estimate is to assume that the effective sampling

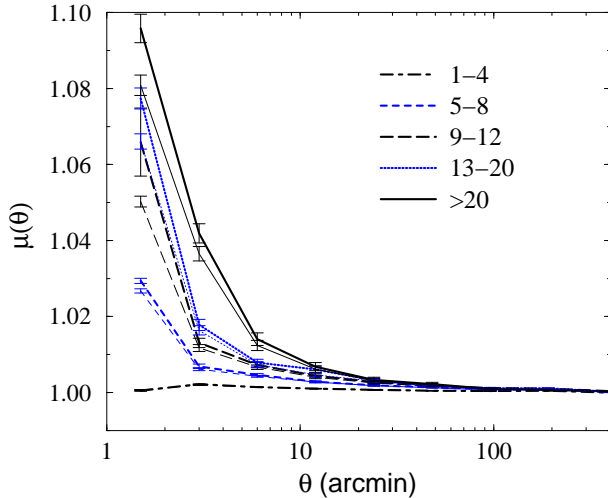


**Figure 5.** Average magnification around mock galaxy groups. The number ranges in the legend are the number of galaxies for the sets of groups. Thick lines include departures from the weak lensing approximation, and thin lines are the weak lensing approximation for the magnification calculation. Errors are the standard deviation of the mean.

used on the simulations is given by the density of cells ( $1 \text{ arcmin}^{-2}$  for our grid), and in a real observation it is given by the background source density. This would yield for the study case adopted here, which has a QSO sky density  $\rho_{QSO} = 43 \text{ deg}^{-2}$ , a factor  $\sqrt{\rho_{\text{cell}}/\rho_{QSO}} = 9$  larger for the magnification error bars.

The magnification alters the light flux  $S$  from sources, which implies that if  $\mu > 1$  a source that could be too faint to be observed in a magnitude-limited survey may be brought to view. The number density of sources in the magnitude limited survey is  $N(> S/\mu)$ . But at the same time the magnification also alters the area behind a lens,  $A' = A/\mu$ , so in a  $\mu > 1$  region the area behind the lens is expanded and the source counting density is diluted. These two competing effects are compared in the net enhancement factor

$$q \equiv \frac{A' N(> S/\mu)}{A N(> S)} . \quad (11)$$

If the source cumulative number counts by flux is of the form  $N(> S) \propto S^{-s}$  then the enhancement factor reduces to  $q = \mu^{s-1}$ . The coefficient  $s$  of the number-flux relation relates to the coefficient of the number-magnitude relation by  $s = 2.5\beta$ . We use  $\beta = 0.29$  where required (Myers et al 2003).

The enhancement can be estimated as the ratio of the the observed number of QSO-group pairs,  $DD(\theta)$ , to the expected number of random pairs,  $DR(\theta)$ . If we recall the cross-correlation estimator

$$\omega_{qg}(\theta) = \frac{DD(\theta)}{DR(\theta)} - 1 , \quad (12)$$

then

$$\omega_{qg}(\theta) = \mu(\theta)^{s-1} - 1 . \quad (13)$$

Figure 6 shows the QSO-group correlation function for groups with different galaxy membership. A departure from weak gravitational lensing is illustrated for groups with more

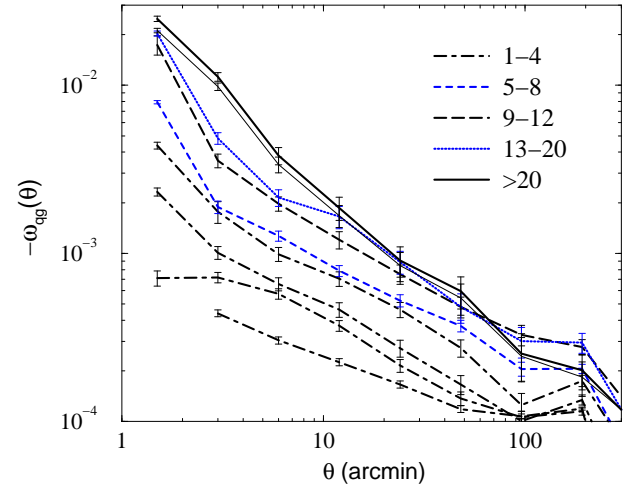


**Figure 6.** Cross-correlation between QSO and mock galaxy groups (we plot  $-\omega_{qg}$  to allow the use of logarithmic scale). The number ranges in the legend are the number of galaxies for the sets of groups. Thick lines include departures from the weak lensing approximation, and thin lines are the weak lensing approximation for the magnification calculation. Curves for groups of membership 1 to 4 are shown individually (from bottom to top for low to high membership). Errors are the standard deviation of the mean.

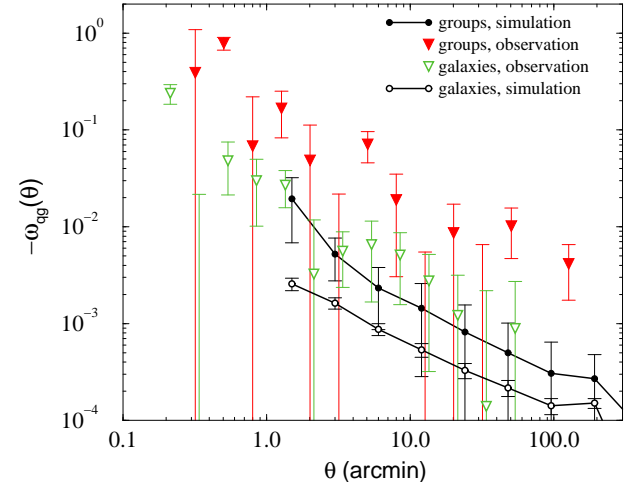


**Figure 7.** QSO-galaxy and QSO-group cross-correlation. Observational data is from Myers et al. 2003 and 2004 with field-to-field errors. Simulation uses groups with 9 or more galaxies and estimated error with same source density as observed data. Some observational points fall below the shown logarithmic scale

than 20 members. The curves show a strong dependence in relation to group membership, indicating its relation to the underling mass overdensity.

Figure 7 compares the cross-correlation results from simulations to data from Myers et al. (2003) for groups, and Myers et al. (2004) for galaxies. Simulation results for angles smaller than 1 arcmin cannot be obtained due to limited simulation resolution; however for angles from 1 to 100 arcmin the comparison with data gives a large disagreement between the amplitudes of observed and simulated cross-correlations.

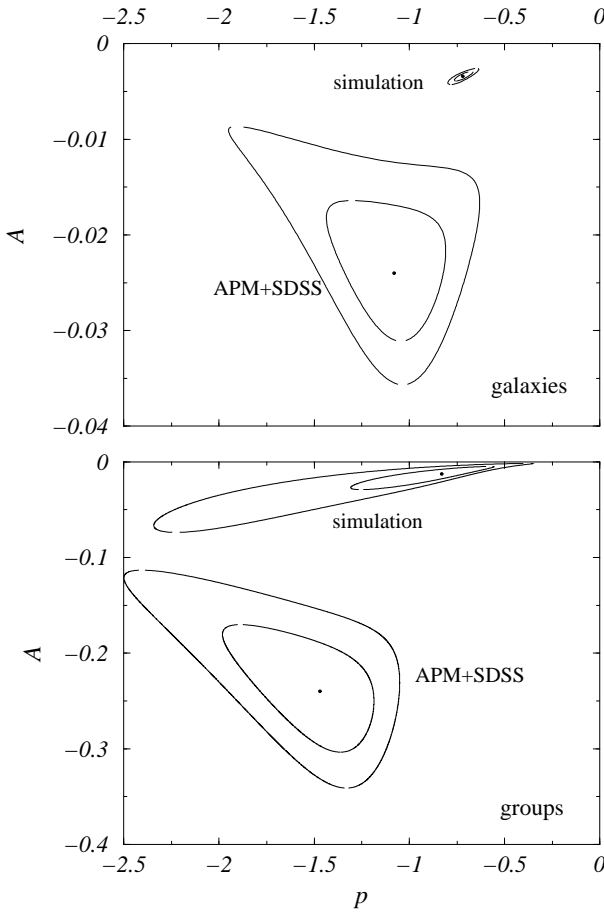


**Figure 8.** Best power law fit,  $1\sigma$  and  $2\sigma$  confidence contours for QSO-galaxy (top panel) and QSO-group (bottom panel) cross-correlation:  $\omega_{qg}(\theta) = A(\theta/1\text{arcmin})^p$ . The least-squares fitted data are the same as shown in Figure 7.

We find the parameters of a power law that best describe the observed and simulated QSO-galaxy and QSO-group cross-correlations. Figure 8 displays these results and the  $1\sigma$  and  $2\sigma$  confidence contours, which shows evidence for a strong disagreement in amplitude between the observed and simulated results, being larger for groups (factor of  $\sim 20$ ) than for galaxies (factor of  $\sim 7$ ). The errors in the cross-correlation data are roughly proportional to the amplitude of the signal, therefore the area inside the confidence contours for the simulation results are considerably smaller than for the observational results.

## 5 ANALYTIC CROSS-CORRELATION

The expression (12) for the cross-correlation is equivalent to (see Appendix A)

$$\omega_{qg}(\theta) \equiv \left\langle \left[ \frac{n_q(\phi)}{\bar{n}_q} - 1 \right] \left[ \frac{n_g(\phi + \theta)}{\bar{n}_g} - 1 \right] \right\rangle, \quad (14)$$

where  $n_q$  and  $n_g$  are the QSO and galaxy (or galaxy group) densities (a bar over a quantity indicates its mean value), and  $\langle \dots \rangle$  represents the average over  $\phi$  and the direction of  $\theta$  (but not its modulus).

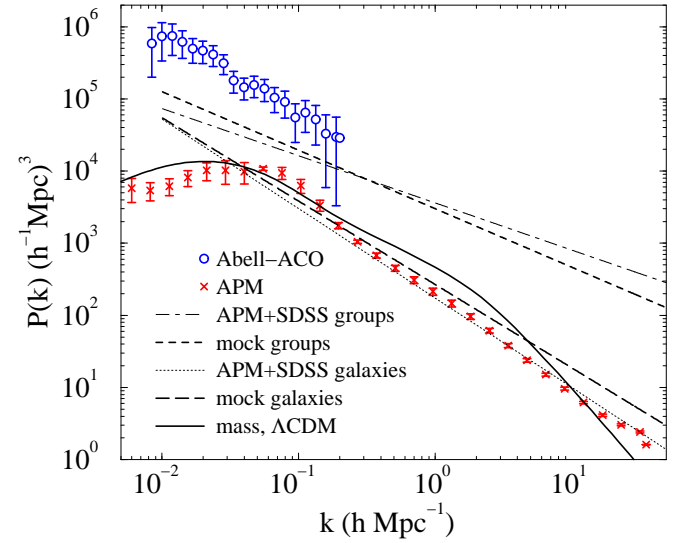


**Figure 9.** Power spectra for galaxies, groups, and mass distribution. The mass power spectrum is for a concordance model. The power law spectra for the APM+SDSS and mock catalogue sets are obtained from the respective auto-correlation function using the method described in the text.

From expression (14) one can derive, assuming weak lensing, that

$$\omega_{qg}(\theta) = \frac{(s-1)}{\pi} \frac{3}{2} \left( \frac{H_0}{c} \right)^2 \Omega_m \int_0^{y_\infty} dy \frac{W_g(y) G_q(y)}{a(y)} \times \int_0^\infty dk k P_{gm}(k, y) J_0[f_K(y)k\theta], \quad (15)$$

where  $y$  is the comoving distance, which here parameterizes time ( $y_\infty$  represents a redshift  $z = \infty$ ), and  $k$  is the wavenumber of the density contrast in a plane wave expansion;  $J_0$  is the zeroth-order Bessel function of first kind; and  $f_K(y)$  is the curvature-dependent radial distance ( $= y$  for a flat universe).  $P_{gm}(k, y)$  can be seen as the galaxy-mass cross-power spectrum (Jain et al. 2003), and under some assumptions (Guimarães et al. 2001) may be expressed as  $P_{gm}(k, y) = \sqrt{P_g(k) P_m(k, y)}$ , where  $P_g(k)$  is the power spectrum for galaxies or galaxy groups and  $P_m(k, y)$  is the non-linear time evolved mass power spectrum.

The mass power spectrum  $P_m(k, y)$  for the  $\Lambda$ CDM model can be obtained analytically from the linear theory and the use of the non-linear prescription given by Peacock & Dodds (1996). Figure 9 shows the mass power spectrum at  $z = 0$  obtained by the method described.

To obtain the three-dimensional power spectrum in real space for galaxies and groups  $P_g(k)$  we use the corresponding two-point angular auto-correlation function  $\omega_{gg}(\theta)$  and the relation (Peacock 1991)

$$\omega_{gg}(\theta) = \int_0^\infty dy y^4 \phi^2(y) \int_0^\infty dk \frac{k}{2\pi} P_g(k) J_0(ky\theta), \quad (16)$$

where  $\phi(y)$  is the selection function, normalized such that  $\int y^2 \phi dy = 1$ . If we assume  $\phi \propto y^{1/2} \exp[-(y/y_*)^2]$ ,  $\omega_{gg}(\theta) = B\theta^\beta$ , and that the power spectrum is a power law, then expression (16) can be integrated and inverted, allowing us to find that

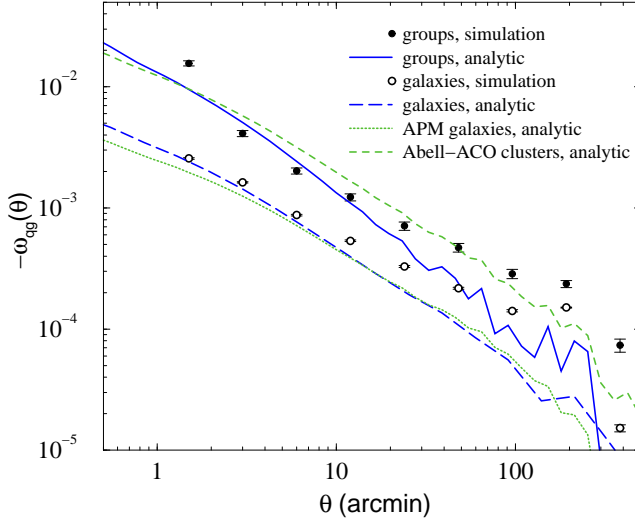


**Figure 10.** QSO-galaxy and QSO-group cross-correlation from simulation and analytic calculation. For the analytic results the only difference in the calculation is the lens (galaxy or group) power spectrum used.

$$P_g(k) = \frac{\pi^3 2^{1+\frac{3}{2}\beta} y_*^{1-\beta} B}{(\beta+2)\Gamma(-\frac{\beta}{2})\Gamma^2(\frac{3}{4})} k^{-(\beta+2)}. \quad (17)$$

We find that  $y_* = 400h^{-1}\text{Mpc}$  allows a good approximation for the selection function used in the generation of the galaxy mock catalogue.

Table 1 contains the best power law fits for the auto-correlation functions for galaxies and groups, and the power spectra that are obtained using equation (17). We plot these spectra on Figure 9, and also the original spectra for APM galaxies (Gaztañaga & Baugh 1998) and Abell-ACO clusters (Miller & Batuski 2001) for comparison.

Figure 10 shows the QSO-galaxy and QSO-group cross-correlation obtained from using Equation (15) and the approximated power spectra for galaxies and groups obtained from the auto-correlation functions, using the method described in this section. There is good agreement between our mass-light simulation method results and the analytic cross-correlation at small angles, which is reassuring for the reliability of our method. However for large angles the analytic cross-correlation is weaker than the simulated. The reason for this discrepancy at large scales is not clear, but one would expect that for angles comparable to the mock sky patch dimensions the simulation results may be unreliable. The steeper curves for the analytic results than for the simulation are in closer agreement with the observational results shown in the last section, since the cross-correlation data from Myers et al. (2003 & 2004) are steeper than the results from the corresponding simulations.

A steeper slope for the QSO-group cross-correlation from the simulation near  $\theta = 1\text{arcmin}$  is probably indicative of the significance of non-linear magnification near the centre of clusters. This effect is not captured by the analytic result because this calculation uses weak gravitational lensing approximations, underestimating lensing in high density regions.

The analytic cross-correlation expression (15) can be further simplified as a power law. If we approximate the

source and lens distributions by Dirac Delta Functions peaked at the average comoving distances ( $\bar{y}_g$  for the QSOs and  $\bar{y}_g$  for the galaxies), and the power spectrum term by  $P(k) = Ak^\alpha$ , then

$$\omega_{gg}(\theta) = \frac{3 \cdot 2^\alpha (s-1)}{\pi} \left( \frac{H_o}{c} \right)^2 \frac{\Gamma(\frac{\alpha}{2} + 1)}{\Gamma(-\frac{\alpha}{2})} \times \frac{f_K(\bar{y}_g) - f_K(\bar{y}_g)}{a(\bar{y}_g)f_K(\bar{y}_g)f_K^{\alpha+1}(\bar{y}_g)} \Omega_m A \theta^{-\alpha-2}, \quad (18)$$

where  $\theta$  is in radians. If one assumes linear bias, then from expressions (18) and (17) it can be deduced that the cross-correlation has the same angular dependence as the galaxy or group auto-correlation, i.e.  $\omega_{gg}(\theta) \propto \theta^\beta$ .

## 6 MASS ESTIMATION

One simple way to estimate the mass of a lens is to assume a mass profile for it, calculate the expected magnification, and use expression (13) to determine the cross-correlation that a population of these lenses would generate (halo lens fitting). One can then find the parameters for the mass profile chosen that best fit the observed QSO-lens cross-correlation, and with it the mass comprised by the lens.

This lens mass estimation method was used by Myers et al. (2003) in groups of galaxies identified in a two-dimensional sky projection, however these groups are not necessarily bound entities. Also, the method essentially assumes that the lenses are identical and isolated objects, ignoring large-scale structure considerations such as clustering and filaments. Nevertheless, the simplicity of the model is appealing, and its result can be attributed to some “effective” halo. Our simulation allows us to test the validity of the method by comparing our mass estimates for lenses obtained from the QSO-lens cross-correlation and directly from the mock matter distribution.

We examine two popular choices for halo profiles, the singular isothermal sphere (SIS) and the NFW profile (Navarro, Frenk and White 1997).

For a SIS halo profile,  $\rho_{\text{SIS}}(r) = \sigma_v/2\pi Gr^2$ , and the mass inside a radius  $r$  is  $M_{\text{SIS}} = 2\sigma_v^2 r/G$ , where  $\sigma_v$  is the velocity dispersion.

For the NFW halo profile

$$\rho_{\text{NFW}}(r) = \frac{\delta_c \rho_c}{(r/r_s)(1+r/r_s)^2}, \quad (19)$$

where  $\rho_c$  is the critical density. We reduce the NFW profile to a one parameter description, the mass inside a  $1.5h^{-1}\text{Mpc}$  radius sphere ( $M_{1.5}$ ), using the relation (Maoz et al. 1997)

$$r_s = 0.3 \left( \frac{M_{1.5}}{10^{15} M_\odot} \right)^\lambda h^{-1}\text{Mpc} \quad (20)$$

where we use  $\lambda = 1/3$ .

The convergence  $\kappa(\theta)$  generated by a halo can be calculated projecting its mass density profile into a plane and using equation (2). The shear can be obtained in this case of circular symmetry by

$$\gamma(\theta) = \bar{\kappa}(\theta) - \kappa(\theta), \quad (21)$$

where  $\bar{\kappa}(\theta)$  is the average value of the convergence inside a radius  $\theta$ . See Wright & Brainerd (2000) for explicit analytical

**Table 1.** Power law representation for auto-correlation functions and power spectra. For the representations in this table  $\theta$  is measured in arcmin and  $k$  is in  $h\text{Mpc}^{-1}$ . The power spectra are in  $h^{-3}\text{Mpc}^{-3}$ .

data set	$\omega_{gg}(\theta)$ fitting range	$\omega_{gg}(\theta)$	$P_{gg}(k)$
APM+SDSS galaxies	0.2–30 arcmin	$(0.34 \pm 0.02)\theta^{-(0.76 \pm 0.01)}$	$1.7 \cdot 10^2 k^{-1.24}$
mock galaxies	1–50 arcmin	$(0.58 \pm 0.05)\theta^{-(0.84 \pm 0.03)}$	$2.6 \cdot 10^2 k^{-1.16}$
APM+SDSS groups	5–50 arcmin	$(10 \pm 2)\theta^{-(1.19 \pm 0.07)}$	$3.0 \cdot 10^3 k^{-0.81}$
mock groups	5–100 arcmin	$(14 \pm 3)\theta^{-(1.35 \pm 0.08)}$	$3.6 \cdot 10^3 k^{-0.65}$

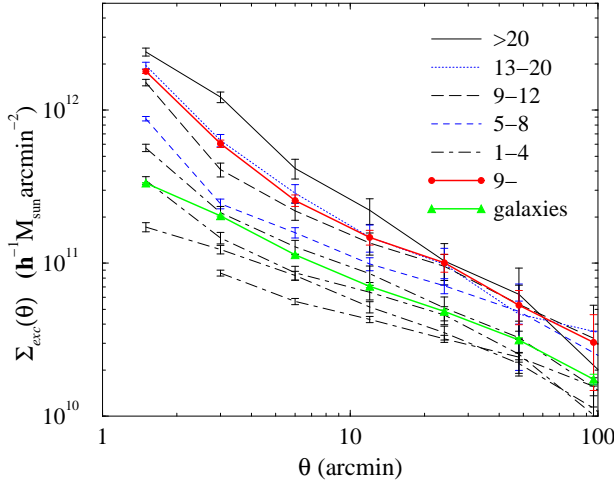


**Figure 11.** Excess surface density  $\Sigma_{exc}$  around galaxies and groups in relation to the mean surface density of the universe to redshift 0.4 ( $4.3 \cdot 10^{12} h^{-1} M_{\odot} \text{arcmin}^{-2}$ ). The legend numbers indicate the galaxy group membership. Errors are the standard deviation of the mean.

expressions for lensing by halos. The magnification can then be calculated using equation (6).

For the galaxies and galaxy groups in our mock catalogue we can estimate the lensing mass associated with them directly from the matter simulation. Figure 11 shows the excess surface density  $\Sigma_{exc}$  in a ring around galaxies and groups in relation to the mean surface density of the universe to redshift 0.4. The excess density is largely insensitive to redshift cuts above this value, since structures above it are not correlated to the luminous structures that we are interested.

The excess mass contained inside a redshift cone centred at a lens (obtained from an integration of the excess surface density) can be used to give an estimate of the average lens mass. However this method in fact includes mass outside the nominal radius, since the cone angular aperture only excludes the mass outside the radius in the perpendicular direction of its axis. The projected mass outside the radius in the line of sight direction is also included. Therefore one would expect the mass obtained through this method to be an over-estimate of the real mass inside a chosen radius. We show these masses around lens centres for cones with angular aperture corresponding to  $1.5h^{-1}\text{Mpc}$  radii for galaxies at an average redshift of 0.15 in Table 2.

Table 2 compares the masses associated with galaxies and groups using halo lens fitting to the simulation and ob-

servational QSO-group cross-correlation results and directly from the matter distribution simulation.

For galaxies the redshift is well defined (to projected galaxy groups it is not) and therefore we can estimate the mass inside a sphere centred on the galaxy coordinates. We calculate this mass for a  $1.5h^{-1}\text{Mpc}$  radius from the centre of the lenses. Such a large radius for a galaxy is chosen to make possible the comparison with similar measures for groups and therefore should be seen as a measure not of the individual galaxies but of the galactic environment.

Looking across the row in Table 2 for the simulation results having galaxies as lens centres, we note that the average mass inside a sphere of radius  $1.5h^{-1}\text{Mpc}$  is roughly six times smaller than the mass computed from the excess surface density. The masses estimated from the simple halo profile lensing models fall between these two. Assuming that the same relation between the described masses applies for groups, then the estimated masses from the halo lens fittings are in reasonable agreement (tending to be an overestimate) with the average real mass associated with groups.

The vertical comparison of the values in the three first columns in Table 2 also reflects the significant amplitude disagreement discussed in Section 4 between observation and simulation, but to a less dramatic degree than the power law analysis. For the galaxy results the mass inferred from observations using the halo profile lensing method is  $\sim 5$  times larger than the corresponding results from the simulation, and for groups this same factor is  $\sim 10$ .

## 7 DISCUSSION

We developed and explored a new approach to the problem of gravitational lensing magnification by galaxy and galaxy groups. This approach allowed a more realistic comparison of the expected QSO-galaxy group correlation in the  $\Lambda\text{CDM}$  model to observation results. The method takes into account the large scale structure of the universe, deviations from the weak lensing approximation, and the group identification procedure that is used in galaxy surveys.

The large scale structure of the universe implies that the groups are clustered, and therefore this feature is properly taken in account in our calculations, in contrast to a simpler approach that models lenses as isolated objects, as used by Myers et al. (2003). Nevertheless, this simple approach was shown to be roughly adequate for lens mass estimation. The mass obtained from isolated halo fitting to cross-correlation results obtained using mock galaxies drawn from a suitably biased Hubble Volume simulation are comparable for the

**Table 2.** Estimated average masses within  $1.5h^{-1}\text{Mpc}$  of the galaxy or group centre in units of  $10^{14}h^{-1}\text{M}_\odot$ . The columns are:  $\sigma_v$  is the velocity dispersion for a SIS model and  $M_{1.5,\text{SIS}}$  is the corresponding estimated mass,  $M_{1.5,\text{NFW}}$  is the estimated mass in a NFW profile model,  $M_{1.5,\Sigma_{\text{exc}}}$  is the estimated mass from an integrated excess surface mass density around galaxies or groups at the average redshift  $z=0.15$  (errors are standard deviation from the mean), and  $M_{1.5,\text{sph}}$  is the average mass inside spheres centred at galaxy positions (errors are standard deviation).  $M_{1.5,\Sigma_{\text{exc}}}$  and  $M_{1.5,\text{sph}}$  are clearly only available for simulations. Groups from simulations have 9 or more galaxies and groups from observation have 7 or more members. The observational data sets come from Myers et al. (2003 & 2004).

data set	$\sigma_v$ (km s $^{-1}$ )	$M_{1.5,\text{SIS}}$	$M_{1.5,\text{NFW}}$	$M_{1.5,\Sigma_{\text{exc}}}$	$M_{1.5,\text{sph}}$
galaxy, simulation	$227^{+39}_{-48}$	$0.4 \pm 0.1$	$0.23^{+0.20}_{-0.19}$	$0.64 \pm 0.01$	$0.11 \pm 0.10$
galaxy, observation	$470^{+59}_{-69}$	$1.5 \pm 0.4$	$1.3 \pm 0.5$	—	—
group, simulation	$409^{+46}_{-53}$	$1.1 \pm 0.3$	$1.1^{+0.6}_{-0.5}$	$1.5 \pm 0.1$	—
group, observation	$1156^{+93}_{-327}$	$9^{+3}_{-4}$	$12 \pm 9$	—	—

two halo profiles examined, and the direct mass estimate from the mock matter distribution.

The consideration of the LSS also allows the inclusion of structures that are not connected to the groups, but act as noise generators for lensing measurements. In fact, most of the lensing for distant sources come from structures around half of the way to the observer, and these structures are not connected to the galaxy groups since they are much closer to the observer. This background lensing signal from uncorrelated structures is the main noise source for the lensing signal from structures associated with observable galaxies. The way to circumvent this problem and obtain a reasonable signal-to-noise measurement of the QSO-galaxy cross-correlation is to have a large foreground population. Also, the larger the mean redshift of this lens population, tending to the point of maximum lensing efficiency, the stronger would be the signal-to-noise. In this respect, a high sky density of background sources allows for a better sampling of the magnification field generated by the mass distribution, and therefore a more precise measurement of the QSO-foreground cross-correlation.

Our results for galaxy groups show that there is a strong dependence on the group galaxy membership that is in accord with the calculated mass estimates for these groups. The cross-correlation curves suggest effective mass profiles for the groups that are distinct in amplitude, but comparable in slope, just favouring slightly cuspier profiles for more massive structures.

The results for galaxy groups of membership 1, i.e. isolated (field) galaxies, when compared to the results of the average galaxy suggest an interesting application. Both the QSO-galaxy cross-correlations and the direct mass estimates for the two populations of lenses indicates that the average galaxy is twice as massive as field galaxies. If the galaxy population is large enough, then it could in practice be broken down into smaller sub-sets according to a chosen characteristic and the cross-correlation observation could be used to compare the relative masses of these sub-populations.

Our simulation lacks mass resolution. A higher resolution simulation of the matter distribution at small redshifts would allow a more precise determination of deviations from linearity of the weak lensing approximation. It would also allow the investigation of smaller angular scales, including halo substructure and the magnification closer to the core of galaxies and clusters. It is possible that substructure may make non-linear magnification important even at regions far

from the identified galaxy or galaxy group centre. Therefore a higher mass resolution simulation could yield a stronger expected cross-correlation due to non-linear lensing, not only for small  $\theta$  but also for larger angles. This effect is worth further investigation.

Our method of calculating lensing maps could also be applied to a broader range of lensing studies, and a natural development would be to include the expected shear map, which would also improve the magnification calculation in high density regions.

The persisting discrepancy between the amplitude of the expected QSO-galaxy and QSO-group cross-correlations in relation to the much lower values expected from the cosmological and lensing models adopted is a stimulus for further investigations.

It may be possible that there are observational issues that cause a systematic error in the cross-correlation determination. The hypothesis of dust is by now very weakened, since the reddening of lensed QSO was found not to be significant by Myers et al. (2003), and the strong positive cross-correlation measured by some groups when using bright QSOs also argues against it. The dust would need to obscure only faint QSOs and cause no reddening to be a viable explanation.

On the other hand, if all the observational issues are very well understood, and the cross-correlation signal due to lensing is stronger than predictions such as we provide in this paper, then various possibilities are indicated. One possibility is a higher mass density for the universe, which would increase the overall weighting of the lenses (the lensing factor). This possibility is highly constrained from other, probably more precise and accurate determinations of  $\Omega_m$ . Another possibility is that the lenses themselves (galaxies and clusters) are more massive than the  $\Lambda\text{CDM}$  model predicts. A third option is that the lensing efficiency is higher than expected from our simulation or analytical calculations that assume weak lensing due to a more prominent role of non-linear lensing. At high density regions (near the core or due to substructure) the magnification is very non-linear and could in principle give a higher contribution to the signal than what is currently being simulated.

## ACKNOWLEDGMENTS

We thank Shaun Cole for assistance with the Hubble Volume Simulation output and galaxy mock generation, and Phil Outram for useful discussions and comments.

## REFERENCES

Barber A.J., Taylor A.N., 2003, MNRAS, 344, 789  
 Bartelmann M., Schneider P., 2001, Phys. Rep. 340, 291  
 Baugh C.M., Efstathiou G., 1993, MNRAS, 265, 145  
 Cole S., Hatton S., Weinberg D.H., Frenk C.S. , 1998, MNRAS, 300, 945  
 Croom S.M., Shanks T., 1999, MNRAS, 307, L17  
 Croom S. M., Smith R. J., Boyle B. J., Shanks T., Miller L., Outram P. J., Loaring N. S., 2004, MNRAS, 349, 1397  
 Frenk C.S. et al., 2000, astro-ph/0007362  
 Gaztañaga E., 2003, MNRAS, 589, 82  
 Gaztañaga E., Baugh C.M., 1998, MNRAS, 294, 229  
 Guimarães A.C.C., Van de Bruck C., Brandenberger R.H., 2001, MNRAS, 325, 278  
 Jain B., Scranton R., Sheth R.K., 2003, MNRAS, 345, 62  
 Jain B., Seljak U., White S., 2000, ApJ, 530, 547  
 Maddox S. J., Efstathiou G., Sutherland W. J., Loveday J., 1990, MNRAS, 243, 692  
 Maoz D., Rix H.W., Gal-Yam A., Gould A., 1997, ApJ, 486, 75  
 Miller C.J., Batuski D.J., 2001, ApJ, 551, 635  
 Myers A.D. et al., 2003, MNRAS, 342, 467  
 Myers A.D. et al., 2004 (*in preparation*)  
 Myers A.D., 2003, PhD thesis, University of Durham  
 Wright C.O., Brainerd T.G., 2000, ApJ, 534, 34  
 Peacock J.A., 1991, MNRAS, 253, 1P  
 Peacock J.A., Dodds S.J., 1996, MNRAS, 280, L19  
 Stoughton et al., 2002, AJ, 123, 485  
 Takada M., Hamana T., 2003, MNRAS, 346, 949  
 Turner E. L., Gott J. R., 1976, ApJ, 32, 409  
 Vale C., White M., 2003, ApJ, 592, 699

## APPENDIX A: CROSS-CORRELATION DEFINITION AND ESTIMATOR

Here we show the equivalence between expressions (12) and (14) for the angular cross-correlation between elements belonging to two populations.

We can describe the populations of objects by two sets of position vectors  $\alpha_i$  ( $i = 1, N_\alpha$ ) and  $\beta_j$  ( $j = 1, N_\beta$ ), where  $N_{\alpha,\beta}$  is the number of elements in either set. So the population density  $n_\alpha$  can be written as

$$n_\alpha(\phi) = \sum_{i=1}^{N_\alpha} \delta_D(\phi - \alpha_i), \quad (A1)$$

where  $\delta_D$  is a Dirac delta function, and the population mean surface density  $\bar{n}_\alpha$  is

$$\bar{n}_\alpha \equiv \langle n_\alpha(\phi) \rangle \equiv \frac{\int n_\alpha(\phi) d\phi}{\int d\phi} = \frac{N_\alpha}{A}, \quad (A2)$$

where  $A$  is the survey area, and a similar expression holds for  $n_\beta$ .

Therefore the cross-correlation between populations  $\alpha$  and  $\beta$  is, according to expression (14),

$$\begin{aligned} \omega_{\alpha\beta}(\theta) &= \left\langle \left( \sum_{i=1}^{N_\alpha} \frac{\delta_D(\phi - \alpha_i)}{\bar{n}_\alpha} - 1 \right) \left( \sum_{j=1}^{N_\beta} \frac{\delta_D(\phi + \theta - \beta_j)}{\bar{n}_\beta} - 1 \right) \right\rangle \\ &= \frac{1}{\bar{n}_\alpha \bar{n}_\beta} \left\langle \sum_i \sum_j \delta_D(\phi - \alpha_i) \delta_D(\phi + \theta - \beta_j) \right\rangle - \frac{1}{\bar{n}_\alpha} \left\langle \sum_i \delta_D(\phi - \alpha_i) \right\rangle - \frac{1}{\bar{n}_\beta} \left\langle \sum_j \delta_D(\phi + \theta - \beta_j) \right\rangle + 1 \\ &= \frac{1}{\bar{n}_\alpha \bar{n}_\beta} \frac{\sum_{ij} \delta_D(\theta - |\beta_j - \alpha_i|)}{2\pi\theta A} - 1 - 1 + 1 \\ &= \frac{DD(\theta)}{DR(\theta)} - 1, \end{aligned} \quad (A3)$$

which is expression (12).

The last step takes two facts into consideration; that  $DD(\theta)$  is the number of pairs of elements from the two populations such that their separation  $|\beta_j - \alpha_i|$  is  $\theta$ , and that for a random distribution of both populations  $DR(\theta) = 2\pi\theta A \bar{n}_\alpha \bar{n}_\beta$ .